Representative galaxy age–metallicity relationships

Andrés E. Piatti,[1,2]★ Antonio Aparicio[3,4] and Sebastián L. Hidalgo[3,4]

[1]*Consejo Nacional de Investigaciones Científicas y Técnicas, Av. Rivadavia 1917, C1033AAJ, Buenos Aires, Argentina*
[2]*Observatorio Astronómico, Universidad Nacional de Córdoba, Laprida 854, 5000 Córdoba, Argentina*
[3]*Instituto de Astrofísica de Canarias, Calle Vía Láctea s/n, E-38200 La Laguna, Tenerife, Spain*
[4]*Departamento de Astrofísica, Universidad de La Laguna, Avda. Astrofísico Fco. Sánchez s/n, E-38206 La Laguna, Tenerife, Spain*

ABSTRACT

The ongoing surveys of galaxies and those for the next generation of telescopes will demand the execution of high-CPU consuming machine codes for recovering detailed star formation histories (SFHs) and hence age–metallicity relationships (AMRs). We present here an expeditive method which provides quick-look AMRs on the basis of representative ages and metallicities obtained from colour–magnitude diagram (CMD) analyses. We have tested its performance by generating synthetic CMDs for a wide variety of galaxy SFHs. The representative AMRs turn out to be reliable down to a magnitude limit with a photometric completeness factor higher than ∼85 per cent, and trace the chemical evolution history for any stellar population (represented by a mean age and an intrinsic age spread) with a total mass within ∼40 per cent of the more massive stellar population in the galaxy.

Key words: techniques: photometric – galaxies: general.

1 INTRODUCTION

The age–metallicity relationship (AMR) has fruitfully been employed to study the chemical evolution of different galactic and extragalactic stellar systems (e.g. Cohen 1982; Catelan & de Freitas Pacheco 1992; Rey et al. 2004). When dealing with the composed stellar population of a galaxy, it has frequently been obtained from the galaxy star formation history (SFH, e.g. Aparicio & Hidalgo 2009; Hidalgo et al. 2011; de Boer et al. 2012; Savino, Salaris & Tolstoy 2015). If such SFHs are extracted from synthetic colour–magnitude diagram (CMD)-based techniques (e.g. Sabbi et al. 2009; VandenBerg, Stetson & Brown 2015), they usually demand the consumption of a lot of CPU time.

In order to be more expeditive in obtaining AMRs from large photometric data bases, Piatti, Geisler & Mateluna (2012) developed a procedure based on the so-called *representative stellar populations*. The method has proved to be useful in comprehensively tracing the AMRs of the Large and Small Magellanic Clouds (LMC/SMC, Piatti 2012; Piatti & Geisler 2013) and that of the Fornax spheroidal dwarf galaxy (Piatti et al. 2014) as well. In this work, we explore the advantages and constraints of such method in obtained astrophysically meaningful AMRs in a more general framework, by applying it to synthetic photometric data sets generated for a wide variety of galaxy SFHs.

In Section 2, we describe the procedure of building galaxy AMRs from their representative stellar populations and compare previous results from this method with those obtained from independent ones. In Section 3, we present different synthetic SFHs used to probe the

ability of the aforementioned technique, while in Section 4 we analyse and discuss its usefulness in different galaxy formation and evolution scenarios.

2 THE REPRESENTATIVE STELLAR POPULATIONS METHOD

Given the CMD of a composed stellar population, Piatti et al. (2012) assumed that the observed main sequence (MS) in any galaxy field is a result of the superposition of MSs with different turn-offs (TOs) and constant luminosity functions (LFs). Hence, the difference between the number of stars of two adjacent magnitude intervals gives the intrinsic number of stars belonging to the faintest interval. Consequently, the biggest difference is directly related to the most populated TO. Geisler et al. (2003) defined this TO as *representative* of a comparatively small field in the sky along the line of sight, and soon after was used by Piatti et al. (2003a,b, 2007), among others, for revealing the primary trends of the stellar composition in different galaxy fields in an efficient and robust way. The definition of a representative TO could not converge to any dominant TO (age) value if the stars in a given field came from a constant star formation rate (SFR) integrated over all time. In such a case, the difference between the number of stars of two adjacent magnitude intervals would result in the same value for any magnitude interval.

The concept of representative TOs is directly applied to AMRs whenever the ages and metallicities used to build them come from representative values, i.e. ages and metallicities estimated by using the photometric information of the prevailing stellar populations. These prevailing populations trace the present-day AMR of a galaxy. They account for the most important metallicity-enrichment

processes that have undergone in the galaxy lifetime. Minority stellar populations not following these main chemical galactic processes are discarded. Therefore, presently subdominant populations in certain locations could have been present in the majority in the galaxy in the past, but were not considered. Note that any AMR built from representative ages and metallicities differs from those derived from modelled SFHs in the fact that it does not include complete information on all stellar populations, but accounts for the dominant population present in each field.

Red clumps (RCs) stars are usually used as standard candles for distance determinations (Paczyński & Stanek 1998; Olsen & Salyk 2002; Subramaniam 2003). However, they are also often used in age estimates based on the magnitude difference δ between the HB/clump and the MSTO for intermediate-age and old clusters (see e.g. Phelps, Janes & Montgomery 1994), since the RC mag is relatively invariant to population effects such as age and metallicity for such stars (Girardi & Salaris 2001). Since the MSTO magnitude is an excellent age indicator, so also is the difference (in magnitude) MSTO − RC. By assuming that the peak of the RC magnitude distribution of a composed stellar population corresponds to the most populous MSTO in the respective field, it is possible to estimate representative ages from composed stellar population CMDs, particularly for ages older than 1 Gyr. For younger ages, the magnitude of the He-burning stage varies with age for such massive stars. Note that this age measurement technique does not require absolute photometry and is independent of reddening and distance as well. An additional advantage is that it is not needed to go deep enough to see the extended MS of the representative stellar population but only slightly beyond its MSTO.

As for the representative metallicities, they can be derived following similar precepts, i.e. by identifying the prevailing stellar population (the more numerous one) in the CMD or Hess diagram of a particular field. For instance, if the position, slope and/or shape of the red giant branch (RGB) is used as a metallicity indicator (e.g. Da Costa & Armandroff 1990; Geisler & Sarajedini 1999; Valenti, Ferraro & Origlia 2004; Choudhury, Subramaniam & Cole 2016), the fiducial placement of the densest RGB path should be considered. Depending on the metallicity sensitivity of the photometric system, particular caveats should be taken into account for those photometric metallicity estimation methods that show some slight dependence with age (Geisler et al. 2003; Ordoñez & Sarajedini 2015).

Piatti (2012) and Piatti & Geisler (2013) built representative AMRs for the SMC and LMC using some 3.3 and 5.5 million stars observed in the Washington CT_1 photometric system, respectively, distributed throughout the main body of each galaxy. The representative MSTO magnitudes turned out to be on average ∼0.6 mag brighter than the mag for the 100 per cent completeness level of the respective fields, so that they actually reached the TO of the representative population of each field. Fig. 1 reproduces their AMRs that trace the main features of the chemical enrichment experienced by these galaxies. Since them, some other independent AMRs have been obtained by Rubele et al. (2012, YJK_s survey) and Bekki & Tsujimoto (2012, theoretical model) for the LMC, and by Cignoni et al. (2013, *HST* photometry) and Rubele et al. (2015, YJK_s survey) for the SMC, among others. Particularly, Rubele et al. (2012, 2015) and Cignoni et al. (2013) used independent procedures to fit synthetic CMDs to the data. They have been overplotted on Fig. 1 for comparison purposes. As can be seen, all of them agree reasonably well.

Piatti et al. (2014) applied also the representative stellar population method to study the AMR of the Fornax dwarf spheroidal
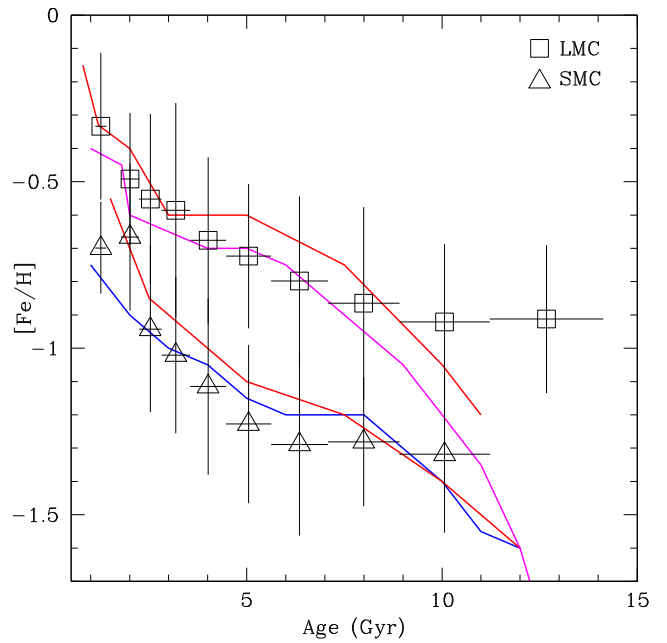
Figure 1. AMRs obtained by Piatti (2012, SMC, open triangles) and Piatti & Geisler (2013, LMC, open boxes) from representative stellar populations. Error bars represent intrinsic dispersion of the representative populations. The AMRs derived by Rubele et al. (2012, 2015, red lines), Bekki & Tsujimoto (2012, magenta) and Cignoni et al. (2013, blue line) are superimposed for comparison purposes.

galaxy from *VI* photometric data obtained with FORS1 at the VLT. According to del Pino et al. (2013), the derived representative *V*(MSTO) mags of each surveyed subregion are brighter than the *V* mag at the 90 per cent completeness level, so that they actually reached the MSTO of the representative oldest populations of the galaxy, particularly in those regions where the oldest populations are indeed the dominant population. When focusing on the most prominent stellar populations, they found that the derived AMRs are engraved by the evidence of an outside-in star formation process and suggested for the first time a possible merger of two galaxies that would have triggered a star formation bursting process that peaked between ∼6 and 9 Gyr ago, depending on the position of the field in the galaxy. Later on, other studies showed similar outcomes (Hendricks et al. 2014; del Pino, Aparicio & Hidalgo 2015; Wang et al. 2016), thus validating the representative stellar population method.

At this point, a question arises unavoidably: since the concept *representative* has associated a specific galaxy tracer (the representative stellar population), we wonder whether there are scenarios in the galaxy formation and evolution for which the *representative* tracer differs from considering as tracers the whole stellar populations. In other words, could the representative AMR be used to describe the global chemical enrichment history of any galaxy? In the subsequent section, we thoroughly examine its scope and constraints.

3 SYNTHETIC AGE–METALLICITY RELATIONSHIPS

3.1 The models

In order to test whether the representative AMRs are robust representations of the most significant age and metallicity present in
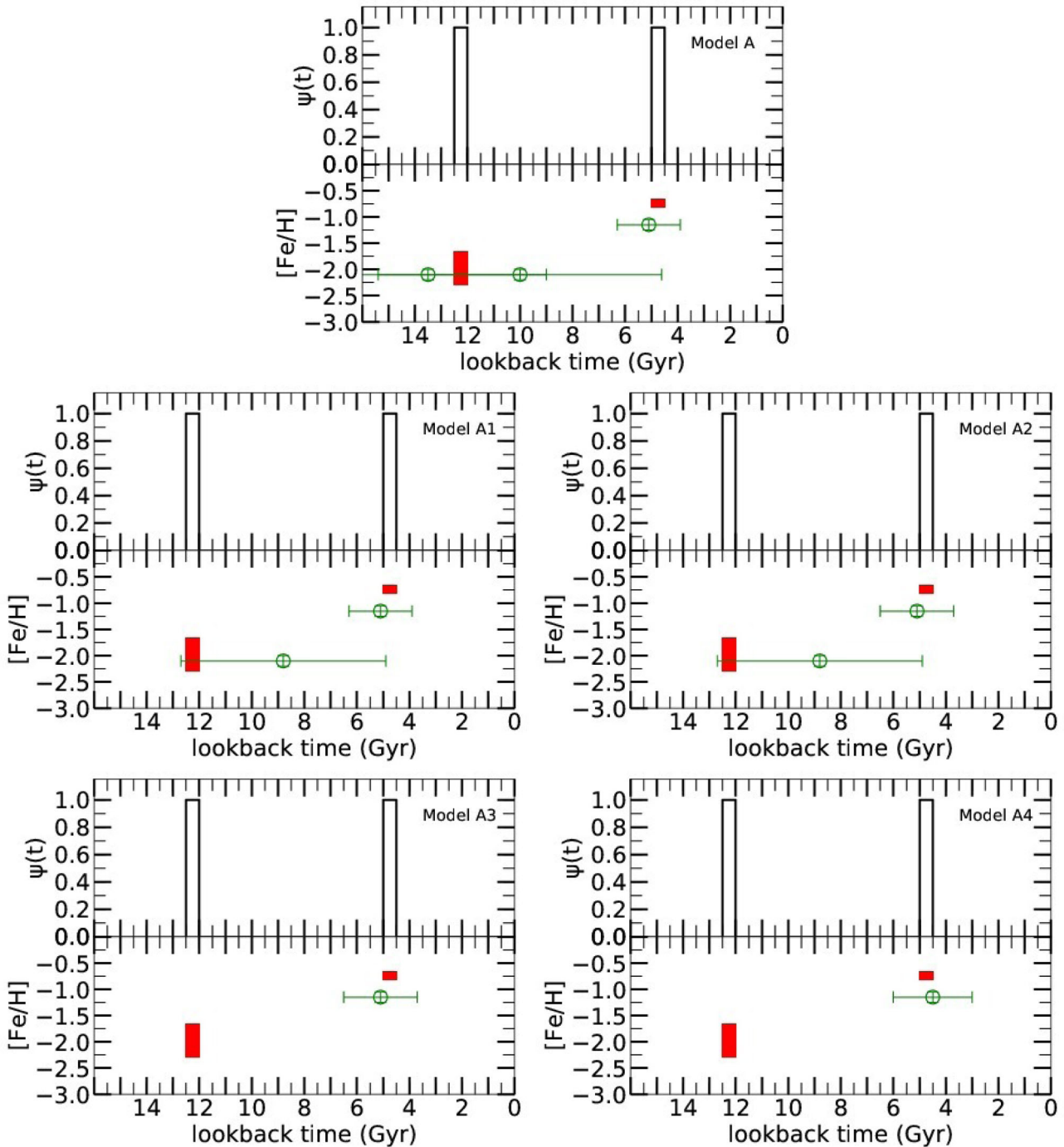
Figure 2. SFH and AMR generated for stellar population model A. To transform Z values to [Fe/H] ones, we used the following relationship: [Fe/H] = log(Z/0.019) (Marigo et al. 2008). The representative AMRs (Table 1) are depicted with open circles for the input model free of observational effects and for the four scenarios obtained varying errors and completeness (see the main text). In all the cases, the upper half panels represent the input SFH of the population model. The bottom half panels show, in red, the input AMR and, in green, the corresponding solutions for the representative AMR.

CMDs we have carried out the following procedure. First, we have generated four synthetic stellar populations with different input SFRs and AMRs; second, we have simulated realistic observational effects in their CMDs, and finally, we have applied the representative AMR method to each of the synthetic CMDs. Comparison of the obtained results and the input data will provide the required information for the robustness test. A short description of the first and second steps follows.

We have used IAC star (Aparicio & Gallart 2004) to compute the four synthetic stellar populations. They have been labelled as A, B, C, D and E and their SFRs and AMRs are shown in Figs 2–6. The characteristics of the populations are as follows: population A consists in two bursts lasting 0.5 Gyr each and starting at ages 12.5 and 5 Gyr, respectively. The metallicity dispersion is used for each one: $0.0001 \leq Z \leq 0.0004$ for the old one and $0.003 \leq Z \leq 0.004$ for the young one. Population B begins with a burst
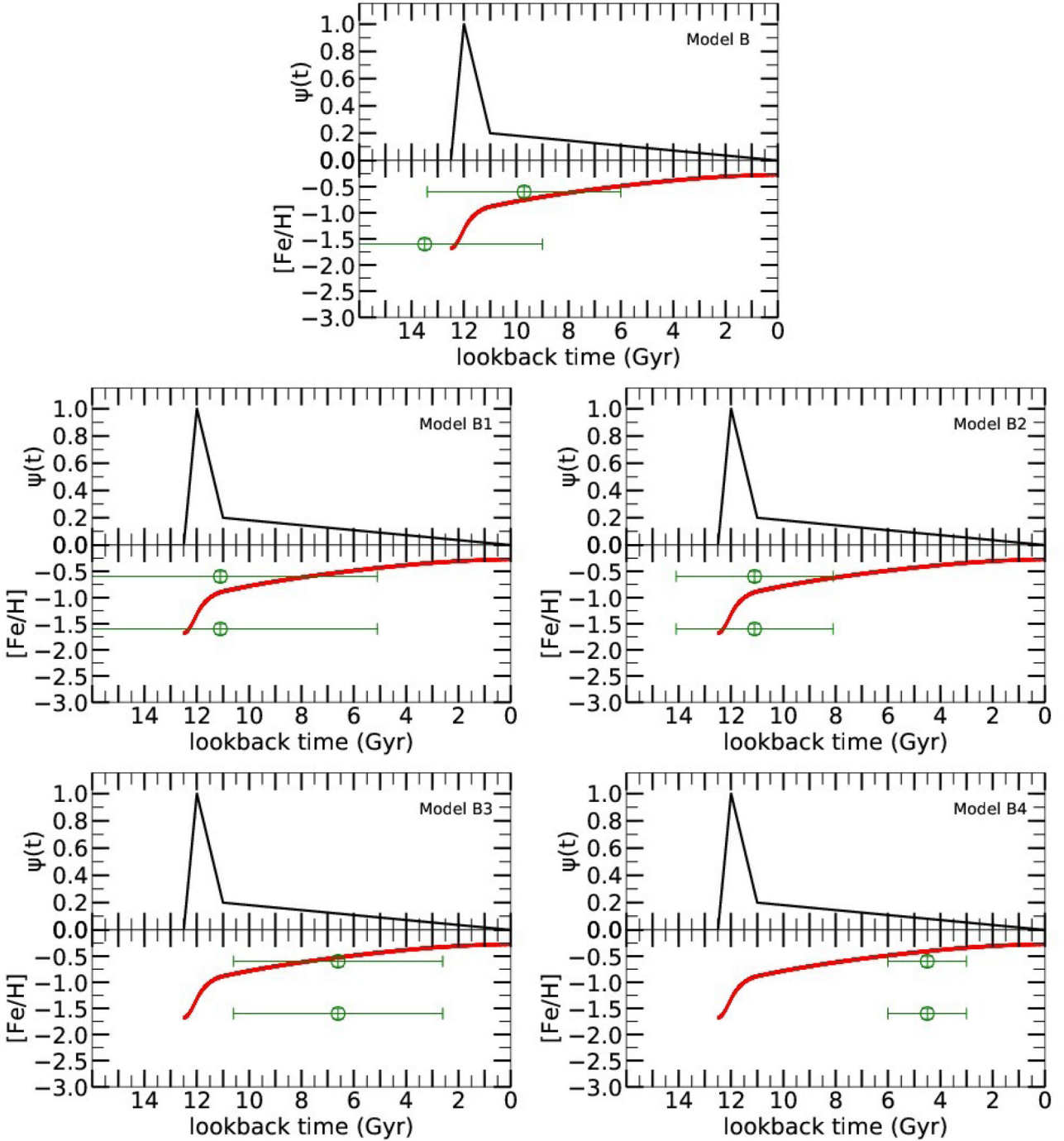
Figure 3. Same as Fig. 2, but for stellar population model B.

that starts at 12.5 Gyr in age, peaks at 12 Gyr and goes down to a low rate at 11 Gyr; after that, the star formation is low and goes on mildly decreasing to 0 at present. The metallicity follows a closed box model with initial value $Z_i = 0.0004$, final value $Z_f = 0.01$ and final gas mass fraction $\mu_f = 0.1$; to this, a Gaussian dispersion has been added such that $\sigma_Z/Z = 0.25$. Population C starts at age 13.5 Gyr with a high SFR that decreases linearly to 0 at present. The metallicity increases linearly from an initial value of $Z_i = 0.0001$ to a final value of $Z_f = 0.01$. As in the former case, a Gaussian metallicity dispersion has been added such that $\sigma_Z/Z = 0.25$. Finally, population D is simply the sum of populations A and

C. In all the cases, a double power law has been assumed for the initial mass function with exponent $x = -1.3$ for the stellar mass interval $0.1 \leq m \leq 0.5$ M$_\odot$ and $x = -2.5$ for the interval $0.5 \leq m \leq 120$ M$_\odot$. Also, a fraction of 30 per cent binary stars has been assumed, with a flat secondary-to-primary mass ratio distribution with minimum value 0.5 and maximum, 1. The number of stars in the M_V versus $(V - I)$ CMD, down to a magnitude limit of $M_I = 5$, has been fixed in 10^5 stars for models A, B and C and 2×10^5 stars for model D. These figures translate in ever formed star masses of $\sim 1.3 \times 10^7$ M$_\odot$ for models A, B and C and $\sim 2.6 \times 10^7$ M$_\odot$ for model D.
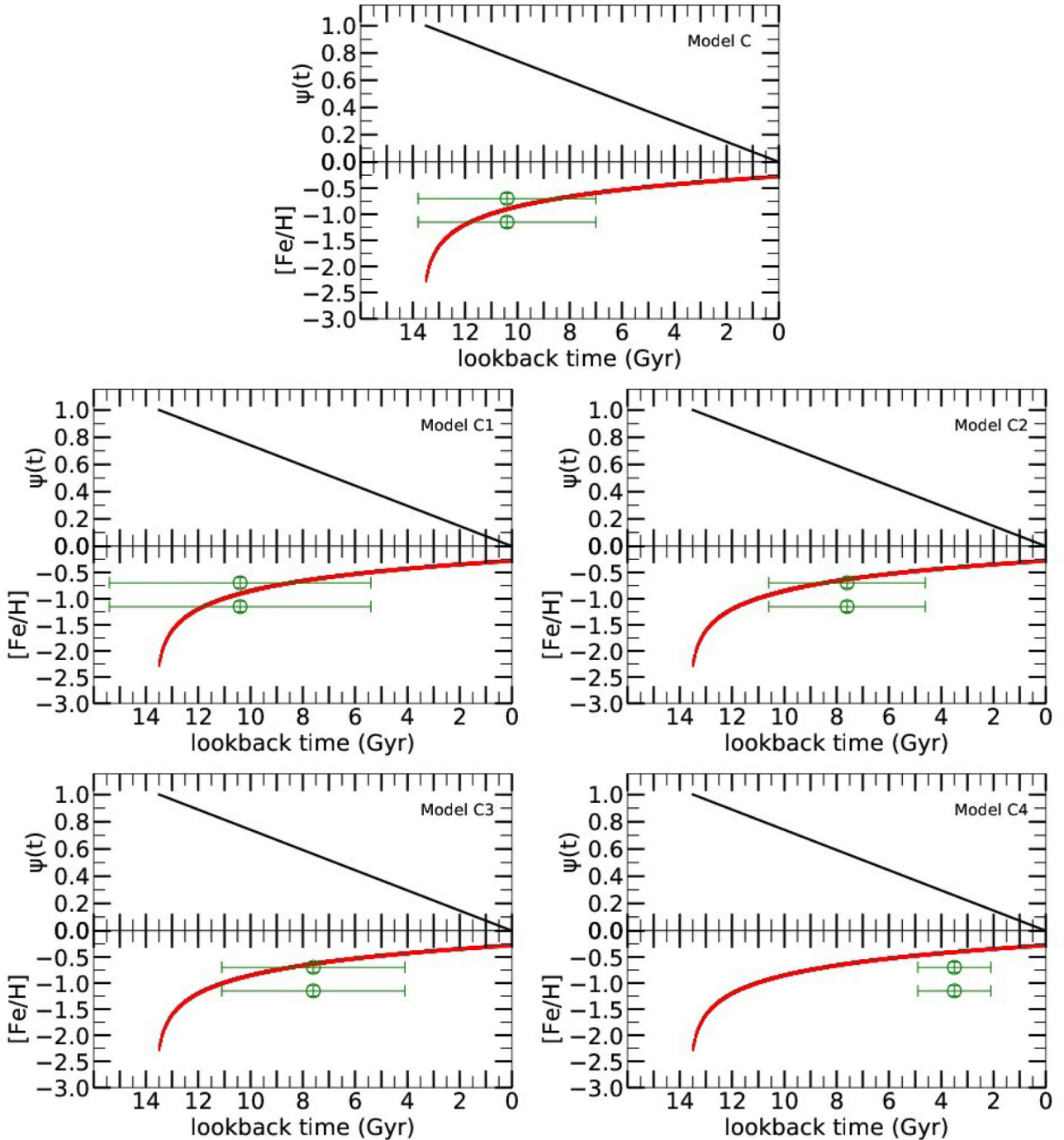
Figure 4. Same as Fig. 2, but for stellar population model C.

Regarding observational effects, four scenarios have been simulated in each population. The corresponding CMDs are labelled from 1 to 4 for each synthetic population; e.g. A1, A2, A3 and A4, for the case of population A. Each scenario is represented by a completeness function and an error distribution. In Fig. 7, completeness as a function of M_V (upper panel) and errors as a function of M_V and M_I (bottom panel) are plotted for the four scenarios. Completeness is simulated in the following way: for each star, the completeness fraction corresponding to its M_V magnitude is obtained. Then, a random number generator is used to maintain or eliminate the star from the photometry list; the star is conserved if the random number is

smaller than the completeness fraction. Errors are simulated in the following way: for each conserved star, shifts in magnitudes in both filters are applied randomly selected from Gaussian distributions which standard deviations are the values of σ_V (plotted in Fig. 7) and σ_I, respectively. In order to illustrate the reader, Fig. 8 depicts some of the generated synthetic CMDs.

3.2 Representative AMRs

Fig. 9 illustrates, as an example, the generated M_V versus $(V - I)_o$ CMD for model B, which includes 100 000 stars. A
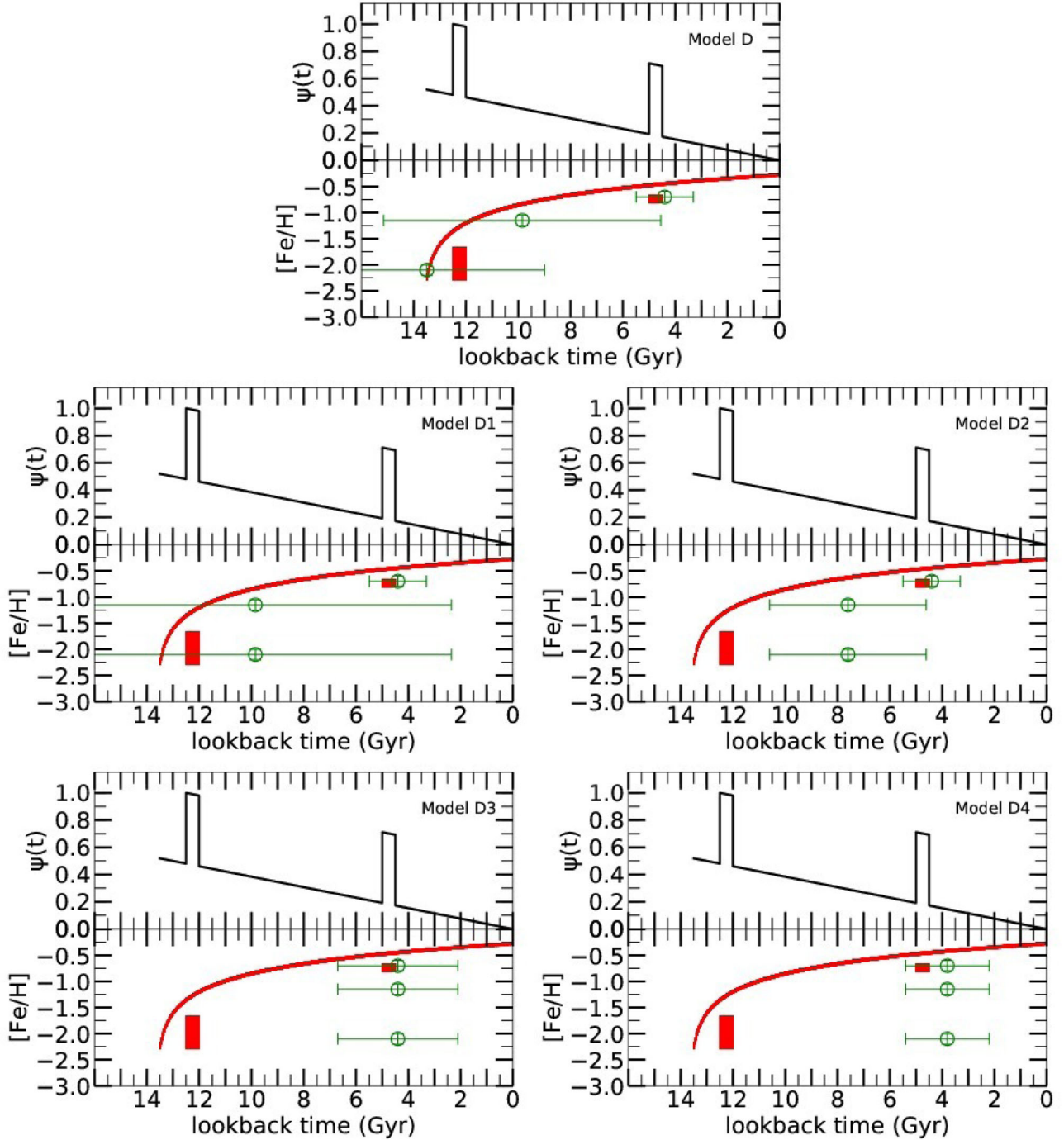
Figure 5. Same as Fig. 2, but for stellar population model D.

mixture of young through old stellar populations clearly appears to be the main feature of this CMD. Other obvious traits presented in the CMD are the populous and broad subgiant branches (an indicator of the evolution of stars with ages (masses) within a non-negligible range), the RCs and the RGBs. In the middle panel of Fig. 9, we drew the respective MS LF. The whole set of MS LFs (one for each model) were obtained by counting the number of stars in M_V bins of 0.25 mag along the MSs, and then they were normalized. The chosen bin size encompasses typical magnitude errors of the stars in each bin, thus producing an appropriate sample of the stars. Note that accurate photometries have magnitude errors for

most of the measured stars usually smaller than 0.20 mag. As is well known, the bin size should be of the order of the uncertainties of the quantity involved to best represent an intrinsic distribution of such a quantity (Piatti 2010, 2011). This means − statistically speaking − that the shape of these LFs are not driven by the chosen bin size.

We then computed for each synthetic CMD the difference between the number of stars of two adjacent magnitude intervals to produce the differential MS LF, as illustrated in the right-hand panel of Fig. 9. As described in Section 2, the peak and the broadness of the differential MS LF provide information about the
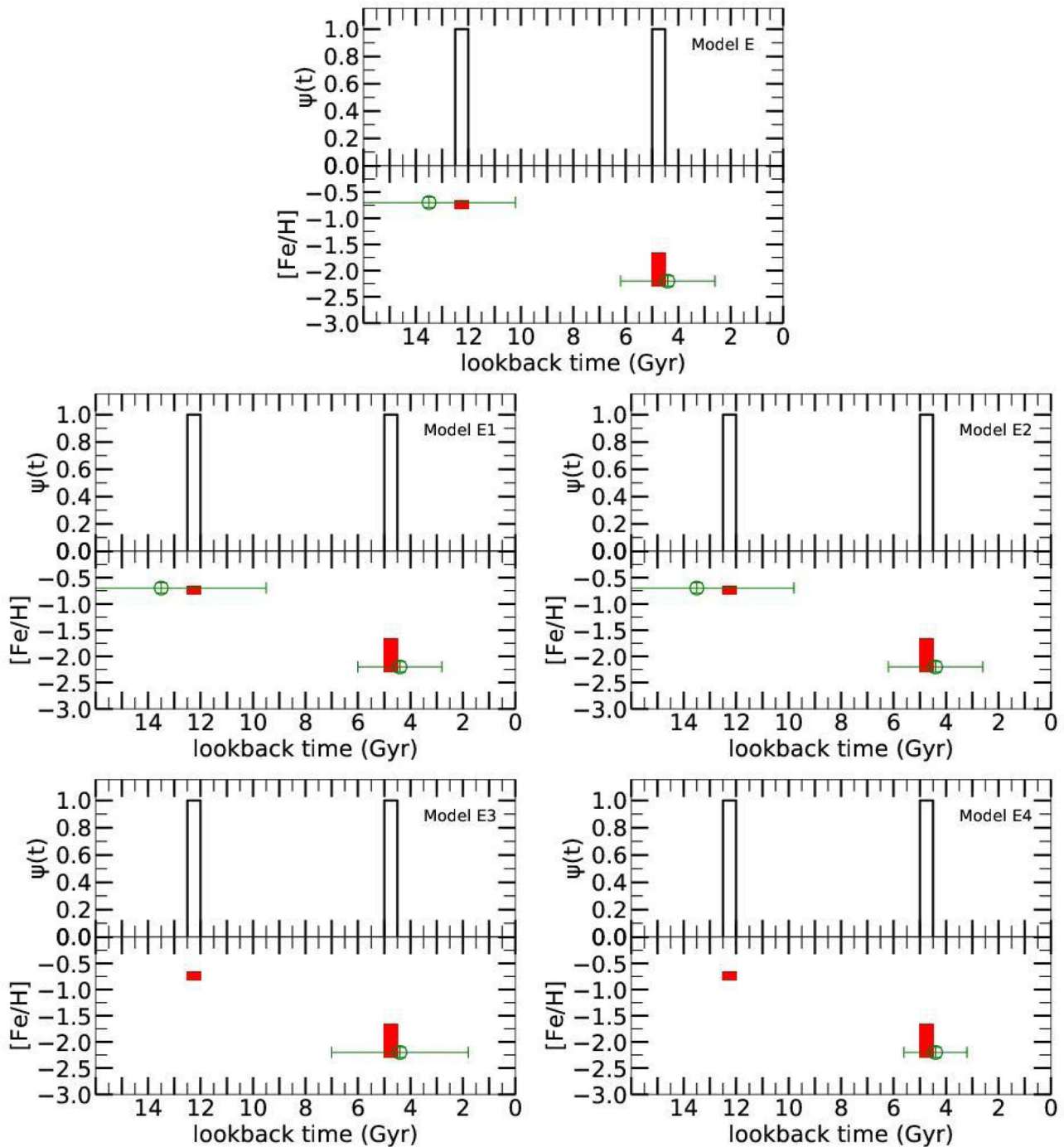
Figure 6. Same as Fig. 2, but for stellar population model E.

representative TO magnitude and its intrinsic width of the considered stellar populations. The prevailing TO (differential MS LF peak) of each synthetic CMD resulted typically ~25 per cent − 50 per cent more populous than the next most dominant population, represented by a secondary peak − sometimes there even could exist a third peak − in the differential LFs. We adopted here the two main peaks we distinguished in the differential MS LFs, as well as their observed full width at half-maximum (FWHMs), as a measure of their intrinsic broadnesses. For the synthetic CMDs of models A, D, D1, D2, D3 and D4, we distinguished three main peaks, whereas for those of models A3 and A4 only one peak. Table 1 lists

the representative M_V(TO) with their associated widths for each modelled SFH.

As for the representative RCs, we built M_V distributions for the RC stars and performed Gaussian fits to derive the mean values and the FWHMs. We performed Gaussian fits using the NGAUSSFIT routine of the IRAF[1] STSDAS package. We adopted a single Gaussian,

---

[1] IRAF is distributed by the National Optical Astronomy Observatories, which is operated by the Association of Universities for Research in Astronomy, Inc., under contract with the National Science Foundation.
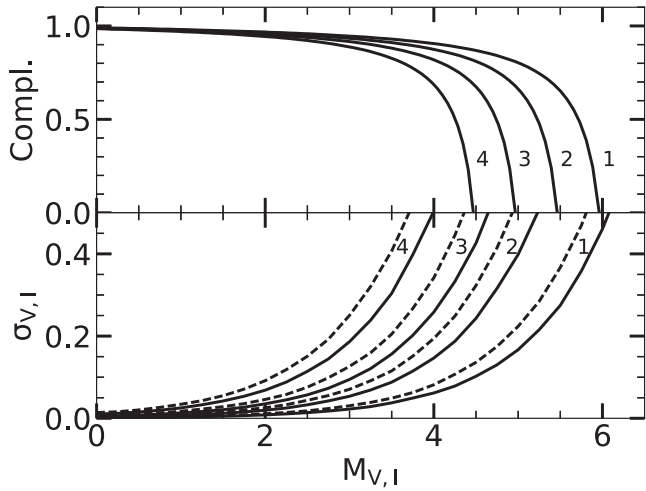
Figure 7. Completeness fraction (upper panel) and errors (lower panel) for the four observational scenarios considered for each stellar population model. In the lower panel, full lines show σ_V versus M_V, while dashed lines refer to σ_I versus M_I.

and fixed the constant and linear terms to the corresponding background levels and to zero, respectively. The centre of the Gaussian, its amplitude, and its FWHM acted as variables. Table 1 lists the resulting representative M_V(RC).

Since we are primarily interested in determining the age and metallicity of the representative star population in each model, we derived δV indices by calculating the difference in the M_V magnitude between the RC and the MSTO. We then derived ages from the δV values by using the equation (Piatti et al. 2014):

$$\text{age(Gyr)} = 0.538 + 1.795\delta V - 1.480(\delta V)^2 + 0.626(\delta V)^3 \quad (1)$$

This equation is only calibrated for ages larger than 1 Gyr, so that we are not able to produce ages for younger representative populations. Table 1 presents the resultant ages and their dispersions. The dispersions have been calculated bearing in mind the broadness of
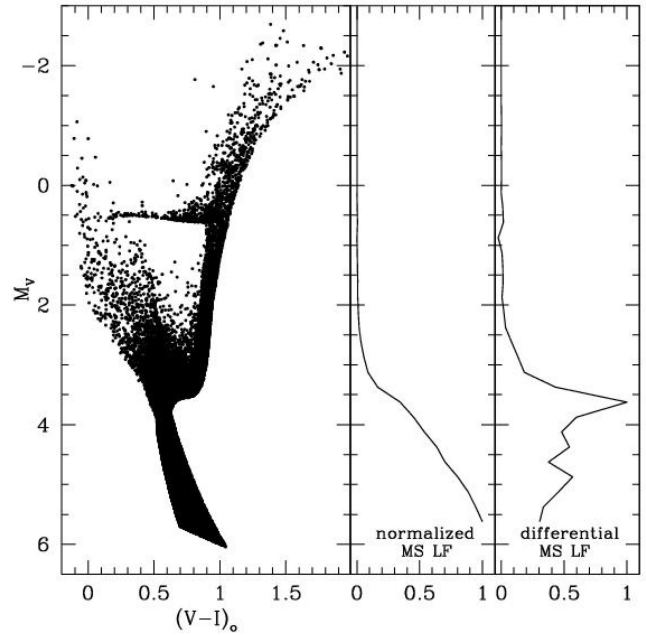
Figure 9. Synthetic M_V, $(V − I)_o$ diagram for model B with the respective normalized MS and differential MS LFs (see the text for details).

the M_V mag distributions of the representative MSTOs and RCs, and represent in general a satisfactory estimate of the age spread around the prevailing population age.

In addition, we also estimated representative metallicities using the equation:

$$[\text{Fe/H}] = -15.16 + 17.0(V − I)_{o,-3} - 4.9(V − I)^2_{o,-3} \quad (2)$$

of Da Costa & Armandroff (1990), once the $(V − I)_o$ colours of the RGB at $M_I = -3.0$ mag and their dispersions were obtained. The $(V − I)_o$ colours were derived from the intersection of the RGBs traced for each model and the horizontal line at $M_I = -3.0$ mag.
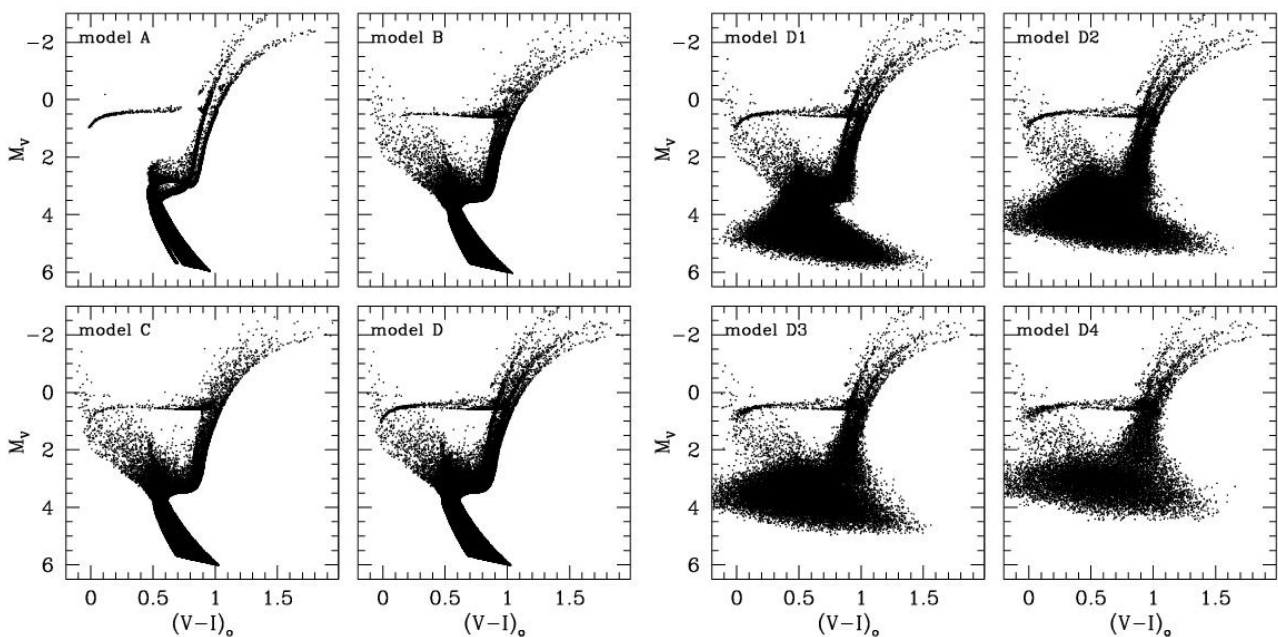
Figure 8. *Left:* synthetic CMDs for models A, B, C and D, without observational effects. *Right:* CMDs for models D for the four different scenarios with observation effects taken into account (see the text for details).

Table 1. Representative parameter values for the generated models.

Model	M_V(TO) (mag)	M_V(RC) (mag)	Age (Gyr)	$(V-I)_{o,-3}$ (mag)	[Fe/H] (dex)
A	2.875 ± 0.200	0.450 ± 0.020	5.1 ± 1.2	1.35 ± 0.02	−1.15 ± 0.1
	3.500 ± 0.500	0.450 ± 0.020	10.0 ± 5.4	1.15 ± 0.02	−2.1 ± 0.1
	4.875 ± 0.400	0.450 ± 0.020	13.5[a]	1.15 ± 0.02	−2.1 ± 0.1
A1	2.875 ± 0.200	0.450 ± 0.020	5.1 ± 1.2	1.35 ± 0.02	−1.15 ± 0.1
	3.375 ± 0.400	0.450 ± 0.020	8.8 ± 3.9	1.15 ± 0.02	−2.1 ± 0.1
A2	2.875 ± 0.250	0.450 ± 0.020	5.1 ± 1.4	1.35 ± 0.02	−1.15 ± 0.1
	3.375 ± 0.300	0.450 ± 0.020	8.8 ± 3.9	1.15 ± 0.02	−2.1 ± 0.1
A3	2.875 ± 0.250	0.450 ± 0.020	5.1 ± 1.4	1.35 ± 0.02	−1.15 ± 0.1
A4	2.750 ± 0.300	0.450 ± 0.020	4.5 ± 1.5	1.35 ± 0.02	−1.15 ± 0.1
B	3.625 ± 0.350	0.600 ± 0.020	9.7 ± 3.7	1.55 ± 0.02	−0.6 ± 0.1
	4.875 ± 0.300	0.600 ± 0.020	13.5[a]	1.25 ± 0.02	−1.6 ± 0.1
B1	3.750 ± 0.600	0.600 ± 0.020	11.1 ± 6.0	1.55 ± 0.02	−0.6 ± 0.1
	3.750 ± 0.600	0.600 ± 0.020	11.1 ± 6.0	1.25 ± 0.02	−1.6 ± 0.1
B2	3.750 ± 0.300	0.600 ± 0.020	11.1 ± 3.0	1.55 ± 0.02	−0.6 ± 0.1
	3.750 ± 0.300	0.600 ± 0.020	11.1 ± 3.0	1.25 ± 0.02	−1.6 ± 0.1
B3	3.250 ± 0.450	0.600 ± 0.020	6.6 ± 4.0	1.55 ± 0.02	−0.6 ± 0.1
	3.250 ± 0.450	0.600 ± 0.020	6.6 ± 4.0	1.25 ± 0.02	−1.6 ± 0.1
B4	2.875 ± 0.300	0.600 ± 0.020	4.5 ± 1.5	1.55 ± 0.02	−0.6 ± 0.1
	2.875 ± 0.300	0.600 ± 0.020	4.5 ± 1.5	1.25 ± 0.02	−1.6 ± 0.1
C	3.675 ± 0.300	0.590 ± 0.020	10.4 ± 3.4	1.50 ± 0.02	−0.7 ± 0.1
	3.675 ± 0.300	0.590 ± 0.020	10.4 ± 3.4	1.35 ± 0.02	−1.15 ± 0.1
C1	3.675 ± 0.450	0.590 ± 0.020	10.4 ± 5.0	1.50 ± 0.02	−0.7 ± 0.1
	3.675 ± 0.450	0.590 ± 0.020	10.4 ± 5.0	1.35 ± 0.02	−1.15 ± 0.1
C2	3.375 ± 0.300	0.590 ± 0.020	7.6 ± 3.0	1.50 ± 0.02	−0.7 ± 0.1
	3.375 ± 0.300	0.590 ± 0.020	7.6 ± 3.0	1.35 ± 0.02	−1.15 ± 0.1
C3	3.375 ± 0.400	0.590 ± 0.020	7.6 ± 3.5	1.50 ± 0.02	−0.7 ± 0.1
	3.375 ± 0.400	0.590 ± 0.020	7.6 ± 3.5	1.35 ± 0.02	−1.15 ± 0.1
C4	2.675 ± 0.350	0.590 ± 0.020	3.5 ± 1.4	1.50 ± 0.02	−0.7 ± 0.1
	2.675 ± 0.350	0.590 ± 0.020	3.5 ± 1.4	1.35 ± 0.02	−1.15 ± 0.1
D	2.875 ± 0.200	0.590 ± 0.020	4.4 ± 1.1	1.50 ± 0.02	−0.7 ± 0.1
	3.625 ± 0.500	0.590 ± 0.020	9.85 ± 5.3	1.35 ± 0.02	−1.15 ± 0.1
	4.875 ± 0.400	0.590 ± 0.020	13.5[a]	1.15 ± 0.02	−2.1 ± 0.1
D1	2.875 ± 0.200	0.590 ± 0.020	4.4 ± 1.1	1.50 ± 0.02	−0.7 ± 0.1
	3.625 ± 0.700	0.590 ± 0.020	9.85 ± 7.5	1.35 ± 0.02	−1.15 ± 0.1
	3.625 ± 0.700	0.590 ± 0.020	9.85 ± 7.5	1.15 ± 0.02	−2.1 ± 0.1
D2	2.875 ± 0.200	0.590 ± 0.020	4.4 ± 1.1	1.50 ± 0.02	−0.7 ± 0.1
	3.375 ± 0.350	0.590 ± 0.020	7.6 ± 3.0	1.35 ± 0.02	−1.15 ± 0.1
	3.375 ± 0.350	0.590 ± 0.020	7.6 ± 3.0	1.15 ± 0.02	−2.1 ± 0.1
D3	2.875 ± 0.450	0.590 ± 0.020	4.4 ± 2.3	1.50 ± 0.02	−0.7 ± 0.1
	2.875 ± 0.450	0.590 ± 0.020	4.4 ± 2.3	1.35 ± 0.02	−1.15 ± 0.1
	2.875 ± 0.450	0.590 ± 0.020	4.4 ± 2.3	1.15 ± 0.02	−2.1 ± 0.1
D4	2.750 ± 0.350	0.590 ± 0.020	3.8 ± 1.6	1.50 ± 0.02	−0.7 ± 0.1
	2.750 ± 0.350	0.590 ± 0.020	3.8 ± 1.6	1.35 ± 0.02	−1.15 ± 0.1
	2.750 ± 0.350	0.590 ± 0.020	3.8 ± 1.6	1.15 ± 0.02	−2.1 ± 0.1
E	2.500 ± 0.250	0.200 ± 0.020	4.4 ± 1.8	1.50 ± 0.02	−0.7 ± 0.1
	3.750 ± 0.200	0.200 ± 0.020	13.5 ± 3.3	1.10 ± 0.02	−2.2 ± 0.1
E1	2.500 ± 0.300	0.200 ± 0.020	4.4 ± 1.6	1.50 ± 0.02	−0.7 ± 0.1
	3.750 ± 0.250	0.200 ± 0.020	13.5 ± 4.0	1.10 ± 0.02	−2.2 ± 0.1
E2	2.500 ± 0.350	0.200 ± 0.020	4.4 ± 1.8	1.50 ± 0.02	−0.7 ± 0.1
	3.625 ± 0.250	0.200 ± 0.020	13.5 ± 3.7	1.10 ± 0.02	−2.2 ± 0.1
E3	2.500 ± 0.500	0.200 ± 0.020	4.4 ± 2.6	1.50 ± 0.02	−0.7 ± 0.1
E4	2.500 ± 0.250	0.200 ± 0.020	4.4 ± 1.2	1.50 ± 0.02	−0.7 ± 0.1

Note. [a]Adopted value due to δV falls outside the range of equation (1).

Table 1 provides with the resulting values and the derived representative metallicities.

4 DISCUSSION AND CONCLUSIONS

In the bottom panels of Figs 2–6, we superimposed the representative ages and metallicities derived in Section 3.2 (green open boxes) to the modelled AMRs (red lines). The error bars represent the intrinsic FWHMs of such representative values. In this section, we compare the trends suggested by the representative age/metallicity values with those coming directly from the modelled SFHs. In other words, we assess how well main changes in the modelled AMRs are detected by the representative AMRs. Note that the representative method is not meant to reproduce any particular modelled stellar population, but to map the main trends in the present-day AMR from the so-called representative populations.

At first glance, there are clear differences in the success with which the representative AMRs represent the actual AMR. For instance, completeness effects constrain significantly the performance of representative AMRs, a result which is expected since representative AMRs come from the employment of observed CMDs with different completeness effects. From the inspection of Figs 2–6, we found that the oldest representative age is highly dependent on this completeness factor. As can be seen, the lower the photometry completeness, the younger the oldest representative age derived. They are in agreement (considering their error bars) with the oldest modelled ages only for models without completeness effect (models A, B, C, D and E) and models with completeness effect 1 and 2, and in some few cases 3. Thus, by entering into Fig. 7 with the absolute magnitude M_V associated to the MSTO of these oldest representative ages (see Table 1), we found that the associated completeness factor is higher than ∼85 per cent. This means that reliable oldest representative ages can be obtained for stellar populations with a photometry completeness higher than ∼85 per cent. Dominant stellar populations observed with less complete photometry do not come up as representative ones. This is somehow an expected result, since it would be hardly possible to say anything about a prevailing stellar population if it were not observed mostly complete. Indeed, the representative AMRs built by Piatti (2012), Piatti & Geisler (2013) and Piatti et al. (2014) for the SMC, LMC and the Fornax dwarf spheroidal, respectively, were obtained from photometry with completeness factors higher than 90 per cent, and hence the good agreement seen with other independent AMRs.

As for the metallicities, we found that the representative AMRs were able to reasonably account for the modelled metallicity enrichment ranges when they arose as a consequence of a bursting formation event (models A, B, D and E). Particularly, the metal-poor ends were mostly well reproduced, while the metal-rich one resulted ∼0.3–0.4 dex more metal-poor. The latter could be due to a relatively low-metallicity sensitivity of the employed photometric system towards the metal-rich end. This does not happen, for instance, for the Washington photometric system which is more sensitive to metallicity (see Fig. 1). Likewise, the modelled age ranges were more satisfactorily reproduced by the resulting representative age ranges whenever models contained bursting formation events.

During quiescent periods of star formation or periods with a decreasing SFR, as is the case of model C, the representative AMRs provide only with mean values of age and metallicity for all the stars formed at $\Psi(t)$ higher than ∼0.6. This can be easily checked by entering into Fig. 4 with the representative ages (mean values and errors) and interpolate the $\Psi(t)$ one for model C (without completeness effect). This means that detected representative populations consist of any stellar population whose stars are within at least ∼40 per cent of the most massive one in the galaxy. As we mention in Section 2, the definition of a representative TO – and hence of a representative stellar population – could not converge to any dominant TO (age) value if the stars in a given field came from a constant SFR integrated over all time. Likewise, minority stellar populations not following these main chemical galactic processes are discarded. Both nearly constant SFR and minority population effects can be seen in Figs 3–6 (models B, C, D and E), where only main bursts were detected.

On the other hand, we confirm that the representative method is suitable to detect mayor star formation events in the galaxy lifetime, such as bursts of stellar populations. For instance, bursts in models A (at ∼5 and 12 Gyr), B (at ∼12 Gyr), D (at ∼5 and 12 Gyr) and E (at ∼5 and 12 Gyr) are well detected, provided a good photometric completeness. This is because a mayor bursting event can produce a
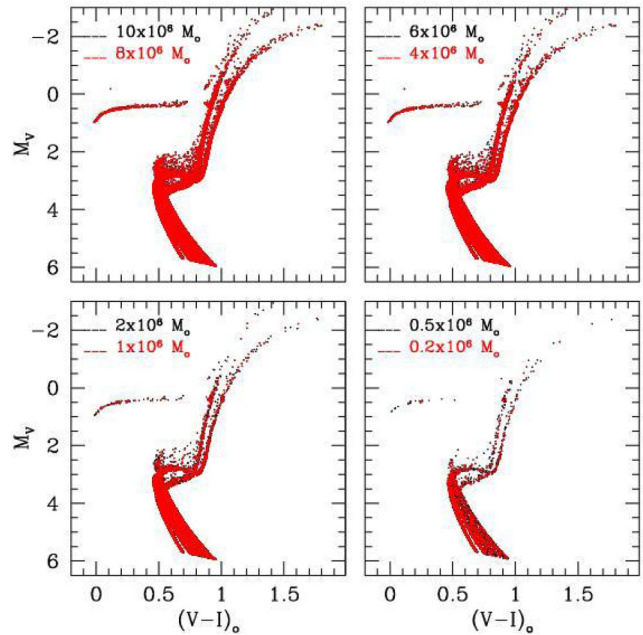
Figure 10. Synthetic M_V, $(V − I)_o$ diagrams for model A for different total galaxy mass, as indicated in each panel.

significant amount of stars (not necessarily followed by a chemical enrichment), and therefore representative populations during the galaxy lifetime can emerge. Moreover, even though the B, C and D modelled AMRs are similar – they consist of an important increase in the metallicity at the very beginning of the galaxy formation and nearly flat curves with a small slope around [Fe/H] ∼ −0.5 dex over most of the galaxy lifetime – the representative AMRs resulted different because of the differences in the SFHs. Those representative AMRs obtained from models with bursting stellar formation events reproduced better the age/metallicity modelled ranges. Successive bursts of star formation could be recognized if the conditions mentioned above about the completeness factor and the $\Psi(t)$ value are fulfilled.

Recovering the dominant stellar population(s), and hence the representative AMRs, depends on the total mass of the galaxy. This is because a representative AMR relies on the composite CMD of the galaxy stellar populations. If real representative MSTOs, RCs or RGBs are not visible in the CMD, the method cannot be employed. To illustrate this point, we generated synthetic stellar populations (synthetic CMDs) with different input total masses for our model A. The resulting synthetic CMDs are shown in Fig. 10. As can be seen, below ∼1–2 × 10^6 M$_\odot$, the redder RGB and the brighter MSTO are difficult to recognize. We then derived representative ages and metallicities for each model and drew Fig. 11 which compares the different outcomes. Once again, the originally modelled AMR (model A) is not recovered for galaxy masses smaller than 1–2 × 10^6 M$_\odot$. For galaxy masses smaller than 0.5 × 10^6 M$_\odot$, the RGB was not detected, so that we could not estimate representative metallicities.

The ongoing surveys of galaxies, e.g. Kelson et al. (2014, CSI), Calzetti et al. (2015, LEGUS) and those for the next generation of telescopes will demand plenty of CPU time to recover a detailed galaxy SFH. This challenge points to the need of expeditive methods for obtaining quick-look AMRs before high-CPU consuming machine codes can be fully executed. The representative method presented here could be of a great help in this respect, providing
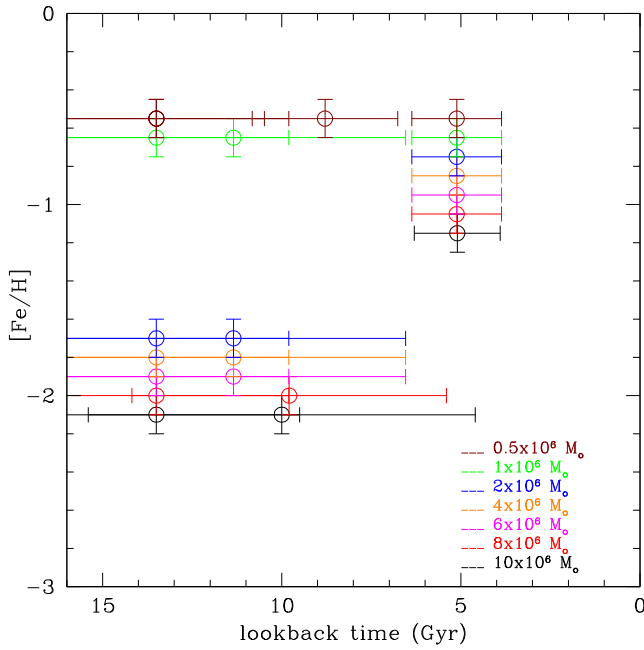
Figure 11. Representative AMRs for model A for different total stellar galaxy mass. We have shifted the points in [Fe/H] to avoid superposition.

AMRs in advance (nearly in real time respect to the availability of observational data) which statistically reflect the most important trends in the galaxy formation and chemical evolution. The representative AMRs turn out to be reliable down to a magnitude limit with a photometric completeness factor higher than ∼85 per cent, and trace the chemical evolution history for any stellar population (represented by a mean age and an intrinsic age spread) with a total mass within ∼40 per cent of the most massive stellar population in the galaxy.

REFERENCES

Aparicio A., Gallart C., 2004, AJ, 128, 1465
Aparicio A., Hidalgo S. L., 2009, AJ, 138, 558
Bekki K., Tsujimoto T., 2012, ApJ, 761, 180
Calzetti D. et al., 2015, AJ, 149, 51
Catelan M., de Freitas Pacheco J. A., 1992, A&A, 258, L5
Choudhury S., Subramaniam A., Cole A. A., 2016, MNRAS, 455, 1855
Cignoni M., Cole A. A., Tosi M., Gallagher J. S., Sabbi E., Anderson J., Grebe E. K., Nota A., 2013, ApJ, 775, 83
Cohen J. G., 1982, ApJ, 258, 143
Da Costa G. S., Armandroff T. E., 1990, AJ, 100, 162
de Boer T. J. L. et al., 2012, A&A, 539, A103
del Pino A., Hidalgo S. L., Aparicio A., Gallart C., Carrera R., Monelli M., Buonanno R., Marconi G., 2013, MNRAS, 433, 1505
del Pino A., Aparicio A., Hidalgo S. L., 2015, MNRAS, 454, 3996
Geisler D., Sarajedini A., 1999, AJ, 117, 308
Geisler D., Piatti A. E., Bica E., Clariá J. J., 2003, MNRAS, 341, 771
Girardi L., Salaris M., 2001, MNRAS, 323, 109
Hendricks B., Koch A., Walker M., Johnson C. I., Peñarrubia J., Gilmore G., 2014, A&A, 572, A82
Hidalgo S. L. et al., 2011, ApJ, 730, 14
Kelson D. D. et al., 2014, ApJ, 783, 110
Marigo P., Girardi L., Bressan A., Groenewegen M. A. T., Silva L., Granato G. L., 2008, A&A, 482, 883
Olsen K. A. G., Salyk C., 2002, AJ, 124, 2045
Ordoñez A. J., Sarajedini A., 2015, AJ, 149, 201
Paczyński B., Stanek K. Z., 1998, ApJ, 494, L219
Phelps R. L., Janes K. A., Montgomery K. A., 1994, AJ, 107, 1079
Piatti A. E., 2010, A&A, 513, L13
Piatti A. E., 2011, MNRAS, 418, L40
Piatti A. E., 2012, MNRAS, 422, 1109
Piatti A. E., Geisler D., 2013, AJ, 145, 17
Piatti A. E., Geisler D., Bica E., Clariá J. J., 2003a, MNRAS, 343, 851
Piatti A. E., Bica E., Geisler D., Clariá J. J., 2003b, MNRAS, 344, 965
Piatti A. E., Sarajedini A., Geisler D., Clark D., Seguel J., 2007, MNRAS, 377, 300
Piatti A. E., Geisler D., Mateluna R., 2012, AJ, 144, 100
Piatti A. E., del Pino A., Aparicio A., Hidalgo S. L., 2014, MNRAS, 443, 1748
Rey S.-C., Lee Y.-W., Ree C. H., Joo J.-M., Sohn Y.-J., Walker A. R., 2004, AJ, 127, 958
Rubele S. et al., 2012, A&A, 537, A106
Rubele S. et al., 2015, MNRAS, 449, 639
Sabbi E. et al., 2009, ApJ, 703, 721
Savino A., Salaris M., Tolstoy E., 2015, A&A, 583, A126
Subramaniam A., 2003, ApJ, 598, L19
Valenti E., Ferraro F. R., Origlia L., 2004, MNRAS, 351, 1204
VandenBerg D. A., Stetson P. B., Brown T. M., 2015, ApJ, 805, 103
Wang M.-Y., Strigari L. E., Lovell M. R., Frenk C. S., Zentner A. R., 2016, MNRAS, 457, 4248

This paper has been typeset from a TEX/LATEX file prepared by the author.